RESEARCH



Comparative characterization of the viscoelastic properties of additive manufacturing polymers

Anil Singh¹ · Mia Chen¹ · George Youssef¹

Received: 30 January 2024 / Accepted: 18 May 2024

© The Author(s), under exclusive licence to Springer Nature B.V. 2024

Abstract

The recent availability of a wide range of additively manufactured materials has facilitated the translation from prototype-limited to application-ready 3D printed components. As such, additively manufactured materials deployed in dynamic environments require extensive characterization to elucidate and optimize performance. This research evaluates the dynamic response of fused filament fabrication and vat photopolymerization printed polymers as a function of temperature. Dynamic mechanical analysis is used to extract the viscoelastic properties of several generations of samples exhibiting a range of thermomechanical behavior, highlighting the stiffness and damping characteristics. A modified stiffness—temperature model supports the experimental characterization and provides additional insight concerning the molecular motion occurring over each thermal transition. The insights from the analysis were collated into a case study that leverages their dynamic characteristics in a multimaterial application. The outcomes from this research assimilate a framework that defines the temperature operating range and broadens the design envelope for these additive manufacturing materials.

Keywords Thermomechanical properties · Fused filament fabrication · Vat photopolymerization · Dynamic mechanical analysis · Stiffness-temperature model

1 Introduction

The emergence of additive manufacturing methods for polymer-based, load-bearing products introduced an influx of printable polymers with a broad range of mechanical properties. Fused filament fabrication (FFF, also called material extrusion, MEX) and vat photopolymerization (VPP) are ubiquitous within current 3D printing technologies due to readily available and versatile polymers. In the former, thermoplastic filaments are heated to a specific temperature to allow the polymer to flow onto the print plate in strategic patterns based on the capabilities of the hardware and the geometry of the printed component. On the other hand, additive manufacturing using VPP hinges on photocurable resins that spontaneously cure in a vat upon exposure to ultraviolet light for a short duration, where the limited

☑ G. Youssef gyoussef@sdsu.edu

Published online: 07 June 2024

Experimental Mechanics Laboratory, Mechanical Engineering Department, San Diego State University, 5500 Campanile Drive, San Diego, CA, 92182-1323, USA



light penetration depth and the relatively rapid set time play a favorable role in accelerating this printing method. While additive manufacturing has attracted assiduous research over the past decade, the focus on the time-dependent properties of printed polymers has been limited. Hence, the primary motivation leading to this research resides in the viscoelastic process–property nexus of additively manufactured polymers using the ubiquitous FFF and VPP processes.

The ubiquity of polymers in additive manufacturing stems from their legacy in net-shape or near-net-shape processing, owing to flexible forms (solid or liquid), relatively low processing temperature (advantageous in FFF), and desirable mechanical properties (Tan et al. 2020; Ligon et al. 2017). The latter include high specific strength-to-weight and stiffness-toweight attributes necessary for consumer goods and high dampening properties required for impact mitigation in sports goods (Prashar et al. 2023; Namvar et al. 2023; Nugraha et al. 2023; Song et al. 2024). However, polymers are more susceptible to loading and environmental conditions than other classes of materials (e.g., metals and ceramics) (Randhawa and Patel 2021; Youssef 2021; Wineman and Rajagopal 2000). For example, the processability of photocurable polymers in the vat photopolymerization 3D printing process is eclipsed by the limited utility in indoor applications since the resin and the realized product exhibit high affinity to extended ultraviolet radiation (Yousif et al. 2023). In other words, deploying photocured polymers in outdoor applications might result in an accelerated reduction in performance, including physical appearance and mechanical properties, due to photo-induced degradation such as photodegradation and photo-oxidation (Yousif et al. 2023; Feng et al. 2023; Riechert et al. 2023). It is well established that extended sun exposure is detrimental to the structural and mechanical behavior of polymers, exemplified by chain sessions of environmentally induced crazing, respectively (Andrady et al. 1998, 2023; Naveen et al. 2023). Anastasio et al. vigorously investigated the interrelationship between processing conditions (light intensity and exposure duration) and the mechanical properties of ultravioletcured methacrylate resin (a common base monomer in many commercially available printable resins) (Anastasio et al. 2019). They reported a monotonic relationship between glasstransition temperature, curing time, and exposure intensity. Furthermore, Anastasio and coworkers revealed that the yield stress directly depended on the curing time and indirectly related to the light intensity. While the study of Anastasio et al. focused on the processing conditions, it amplified the concerns about the interdependence of the long-term behavior on the loading and environmental conditions. Kim et al. ascertained similar results while examining the mechanical behavior of ultraviolet-cured polyester-acrylate resins, reporting the effect of the photo-initiator type and the weight ratio on the tensile strength (Kim and Seo 2004). The properties of polymers, irrespective of the manufacturing process, are timedependent, giving rise to their viscoelastic behavior (Youssef 2021). The latter transpires as a reduction in the stress as a function of time at constant strain (i.e., stress relaxation behavior) or decreasing strain when the load is fixed for an extended duration (i.e., creep response) (Youssef 2021). Such time-dependent properties require an alternative characterization mindset to delineate the process-property interrelationship in the context of the susceptibility of polymers to extended loading durations. Hence, the primary objective of this research is to explore the viscoelastic properties of FFF and VPP printed materials with a broad spectrum of mechanical properties, ranging from compliant to stiff, as discussed in the forthcoming sections.

While the scientific community recognizes that FFF printing is at the forefront of several technological innovations, there has been a notable lag in characterizing the dynamic properties of FFF-produced materials. Interest in the FFF process peaked upon the expiration of the original patent by Stratsys[®], allowing hobbyists and practitioners access to readily



available equipment, software, and materials (Yadav et al. 2023; Kumar et al. 2023). The recent keen effort has resulted in the infiltration of this agile technology into several application domains, including consumer goods, replacement parts in aging and old aircraft, robotics, and sports gear, to name a few prominent examples (Yadav et al. 2023; Ramya and Vanapalli 2016). Nonetheless, only quasistatic testing of these materials has been broadly reported in the literature as a function of printing parameters, including printing orientation, speed, enclosure temperature, and layer height (Bakhtiari et al. 2023; Pachauri et al. 2023; Yankin et al. 2023; Sola et al. 2023). Arguably, the focus on quasistatic characterization paradigms is justified to elucidate the general properties of FFF printed parts and components, instilling confidence in the overall mechanical performance, accelerating the development of end-use products, and shifting away from prototyping (Yadav et al. 2023; Brans 2013). Recently, Cuan-Urquizo and colleagues collated a topical review of the mechanical properties of FFF printed materials and structures, compiling the ongoing experimental, computational, and theoretical approaches reported in the open literature (Cuan-Urquizo et al. 2019). In the review by Cuan-Urquizo et al., they emphasized the structureproperty relationship and the mechanical characterization of FFF structures and materials (Cuan-Urquizo et al. 2019), summarizing the tensile and compressive performance of ABS (acrylonitrile butadiene styrene) (Uddin et al. 2017; Ahn et al. 2002; Rodríguez et al. 2001; Huynh et al. 2020; Youssef et al. 2021; Sood et al. 2012; Onwubolu and Rayegani 2014), Ultem 9085 (polyetherimide) (Zaldivar et al. 2017), PLA (polylactic acid) (Wittbrodt and Pearce 2015; Laureto and Pearce 2018), PEEK (polyether ether ketone) (Deng et al. 2018; Gómez-García et al. 2023), and polycarbonate (Shojib Hossain et al. 2013; Reich et al. 2019; Shojib Hossain et al. 2014; Vidakis et al. 2022). Notably, the flexural, fracture, fatigue, and cyclic loading performances of various FFF printed materials have also attracted significant research attention (Adibeig et al. 2023; Svetlana et al. 2021; Patterson et al. 2021). Collectively, these research studies point to the drastic effect of the FFF printing process on the quasistatic mechanical properties, specifically as a function of the printing orientation due to the layer-to-layer interactions. It is imperative to elucidate the dynamic properties of FFF printed materials, as is the case herein.

The vat photopolymerization additive manufacturing process is the oldest approach used in 3D printing fabrication, using a broad range of resins, and new ones that are easily amendable to tune the mechanical properties are continuously introduced. Generally, a thin layer of photocurable resin is exposed to ultraviolet light to cure, upon which a new layer is introduced, and the process is repeated in a layer-by-layer fashion. The facility of the VPP printing process stems from the readily available photocurable resins and agility in preparing composite resin by adding reinforcing particles or fibers (Malley et al. 2021; Lantean et al. 2022; Wang et al. 2022). Such tunability culminates in research centered around characterization and modeling the mechanical behavior of photocurable, 3D printed resin, accounting for the viscoelastic and hyperelastic responses intrinsic to this class of materials (Xiang et al. 2020). Since VPP printing is done at room temperature, the mechanical properties transcend their FFF counterparts due to the absence of thermal layer adhesion challenges. Dizon et al. collated a recent review summarizing the mechanical properties of VPP-manufactured samples (Dizon et al. 2018; Chantarapanich et al. 2013; Dulieu-Barton and Fulton 2000; Hague et al. 2004). Naik et al. also investigated the process-induced anisotropy at quasistatic loading conditions, arguing the need for dynamic characterization (Naik and Kiran 2018). Brighenti et al. elucidated the tensile and cyclic properties of photopolymerized polymers as a function of ultraviolet exposure and layer thickness at isothermal testing conditions (Brighenti et al. 2023). Finally, Kuenstler et al. explored the dynamic properties of VPPprinted recyclable thermoset films, leveraging dynamic covalent bonds to facilitate conformational rearrangement and plasticity for recyclability and self-healing (Kuenstler et al.



2023). Hence, there needs to be more understanding of the dynamic properties of 3D printable materials, irrespective of the printing process, as a function of temperature, i.e., the leading motivation of this research.

The novelty of this research stems from filling the knowledge gap about the dynamic properties of several common printable polymers using fused filament fabrication and vat photopolymerization with a broad spectrum of mechanical responses. The FFF materials include thermoplastic polyurethane (TPU), acrylonitrile butadiene styrene (ABS), and carbon-reinforced nylon filaments (CFN), while the VPP resins are flexible rubber-like and stiff ABS-like resins. Upon printing and conditioning, the samples were characterized using the dynamic mechanical analyzer in a dual-cantilever configuration as a function of temperature at a single frequency. The results ascertain the importance of dynamic characterization in fully deciphering the behavior of the 3D printed materials in realistic loading conditions. These results unlock the potential of additively manufactured products using the FFF and VPP processes while accelerating the bench-to-market development cycle.

2 Materials and methods

To holistically account for the variance in material properties between the many polymers employed in current FFF and VPP additive manufacturing printing strategies, representative materials that embody elastomeric and brittle material responses were chosen from options available for each approach. Three FFF filaments were selected, including thermoplastic polyurethane, acrylonitrile butadiene styrene, and chopped carbon fiber-reinforced nylon. Thermoplastic polyurethane (TPU, red Fiberflex 40D, Fiberology) filament exhibits highly elastic, rubber-like properties, leading to a range of applications such as prosthetics and orthotics, sporting equipment, plumbing, and medical equipment (Senna 2019; Sărăndan 2022; Desai et al. 2023). Acrylonitrile butadiene styrene (ABS, generic filament) is a resilient thermoplastic polymer, ubiquitous in conventional and advanced manufacturing of computer monitors, Lego® bricks, keyboard caps, and home appliances (Anandhan et al. 2003; Sabatini et al. 2023; Gurjar et al. 2018). The final filament material is a composite of chopped carbon fiber and nylon matrix (CFN, black CF-NYLON G3, CARBONX), exhibiting desirable physical and mechanical properties suitable for industrial applications (Alarifi 2022).

The geometries of all FFF samples were configured for printing using Ultimaker Cura 5.2.1 (an open-source slicing software) with a 0.12 mm layer height, three perimeter layers, and 100% diagonal infill within the flat face, as shown in **Fig. 1**. The figure also shows the dimensions of the rectangle samples, 60 mm long \times 12.5 mm wide \times 1.6 mm thick, used for dynamic testing, as discussed next. All samples were printed individually at the center of the print plate to avoid inter-batch variations. To prevent samples from lifting off while printing, a brim of ten layers width was used for build plate adhesion. The printing brim is not part of the final samples used in dynamic testing and was discarded after the samples were removed from the print plate. TPU samples were fabricated on a Creality CR-10 printer with a nozzle temperature of 240 °C and a bed temperature of 60 °C without controlling the printing environment given the open printing enclosure (i.e., printing at ambient conditions). The ABS samples were printed on a Funmat HT printer at 245 °C nozzle temperature and 110 °C bed temperature in a 70 °C heated environment to compensate for the material tendency to shrink and to minimize warping and lifting off the build plate during printing. Finally, the CFN samples were also printed on the Funmat HT printer at a nozzle temperature of 270 °C,



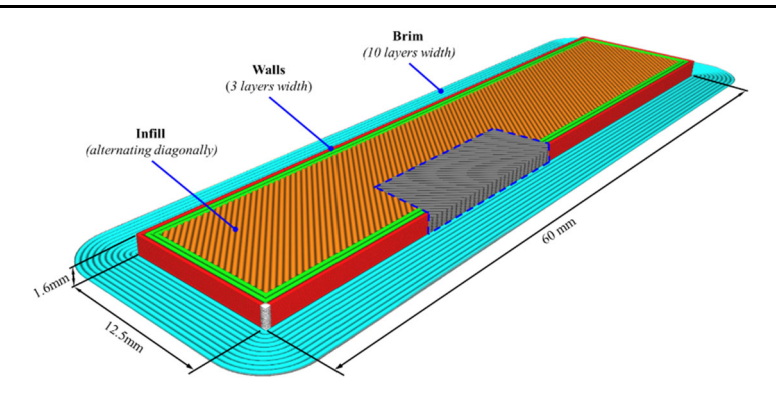


Fig. 1 Sample design and slicing strategy for samples printed via FFF 3D printing process

Table 1 FFF printing temperatures for TPU, ABS, and CFN filaments

Material	Printer	Nozzle Temp (°C)	Bed Temp (°C)	Enclosure Temp (°C)
TPU	Creality CR-10	240	60	27 (ambient)
ABS	Funmat HT	245	110	70
CFN		270	80	70

bed temperature of 80 °C, and an enclosure temperature of 70 °C. **Table 1** summarizes the printing temperatures and equipment used in preparing the samples used in this research.

The VPP samples were fabricated using a Prusa SL1S speed-masked stereolithography printer and post-processed using a Prusa CW1S curing and washing machine. The photocurable resins included black flexible rubber-like resin (F69, Resione) and clear blue ABS-like resin (ABS-Like Photopolymer Resin, ELEGOO). The F69 resin samples were printed using an initial bottom exposure of 60 s for the initial three layers, whereas subsequent layers were printed with a normal exposure time of 15 s and a nominal layer thickness of 50 μm . Three samples were printed concurrently on their flat face in a vertical orientation with respect to the build plate. After printing, the samples were washed twice in the CW1S using water and isopropyl alcohol, where each washing cycle lasted for 3 min. The samples were then dried under a convective air supply at 35 °C for 4 min on each side. Finally, the F69 samples were ultraviolet cured in the CW1S for an additional 4 min on each side. The additive manufacturing of the ABS-like resin samples faithfully followed the same procedure with two modifications. The layer exposure time was reduced to 8 s, and the drying and curing times were shortened to 3 min.

The FFF and VPP samples were mechanically characterized using a dynamic mechanical analyzer (DMA, Q800, TA Instruments Inc.) to investigate the mechanical response of additively manufactured polymers as a function of temperature. The samples were tested in the dual-cantilever clamp configuration (**Fig. 2**), clamping torques listed in **Table 2**, and submitted to a temperature ramp, reporting the storage and loss moduli. All samples were conditioned in a dark ambient environment for nearly 30 days before dynamic mechanical testing. The temperature was initially lowered to -100 °C using liquid nitrogen, and the samples were equilibrated for 5 min to achieve isothermal conditions before the test commenced. Samples were then loaded sinusoidally at a frequency of 0.1 Hz as the temperature



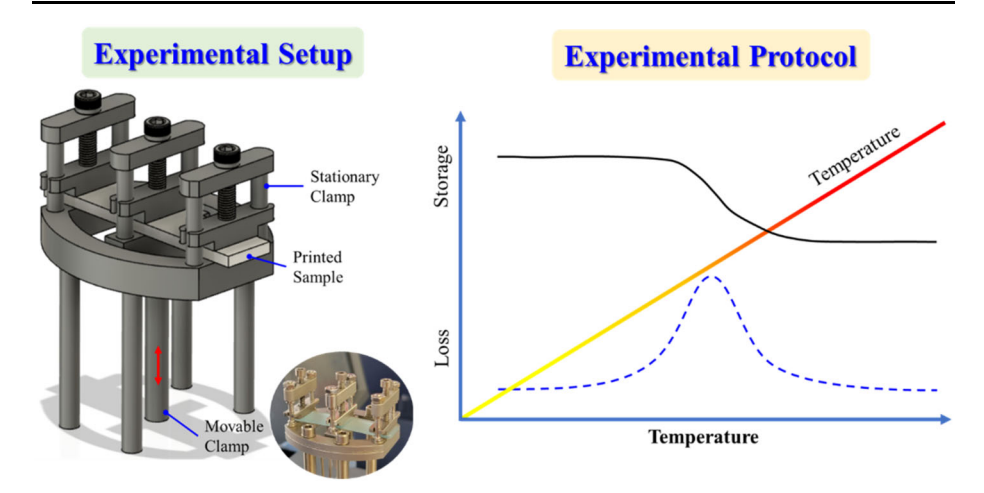


Fig. 2 Dynamic mechanical analysis of 3D printed samples in dual-cantilever beam configuration as function of temperature, showing the (a) setup and (b) protocol

Table 2 Dynamic testing parameters as function of 3D printed materials

Material	Clamping torque (N.m)	Amplitude (μm)
FFF-TPU	0.68	10
VPP-F69 resin		
VPP-ABS-like resin		
FFF-ABS	0.90	15
FFF-CFN		

was ramped from -100 °C to 100 °C at a rate of 3 °C/min, with a 5 min hold at 100 °C at the end of the test cycle before cooling to ambient temperature. The loading amplitude was adjusted based on the printed polymer to avoid premature failure during the cyclic testing paradigm. The clamping torques and loading amplitudes used for each material are listed in **Table 2**.

3 Results and discussion

This section is divided into four subsections. It reports the dynamic thermomechanical responses of FFF and VPP printed materials and synthesizes the data in the context of the mechanics of time-dependent materials.

3.1 Dynamic thermomechanical behavior of FFF printed materials

Fig. 3 reported the storage and loss moduli of three materials printed using the FFF process, including TPU (Fig. 3a), ABS (Fig. 3b), and carbon-reinforced nylon (Fig. 3c), as a function of temperature ranging from -100 °C to the respective terminal point. The figures also show the $tan\delta$ (= E''/E') as a measure of the dampening behavior of these materials (Youssef 2021). As mentioned above, the mechanical responses in Fig. 3 were collected



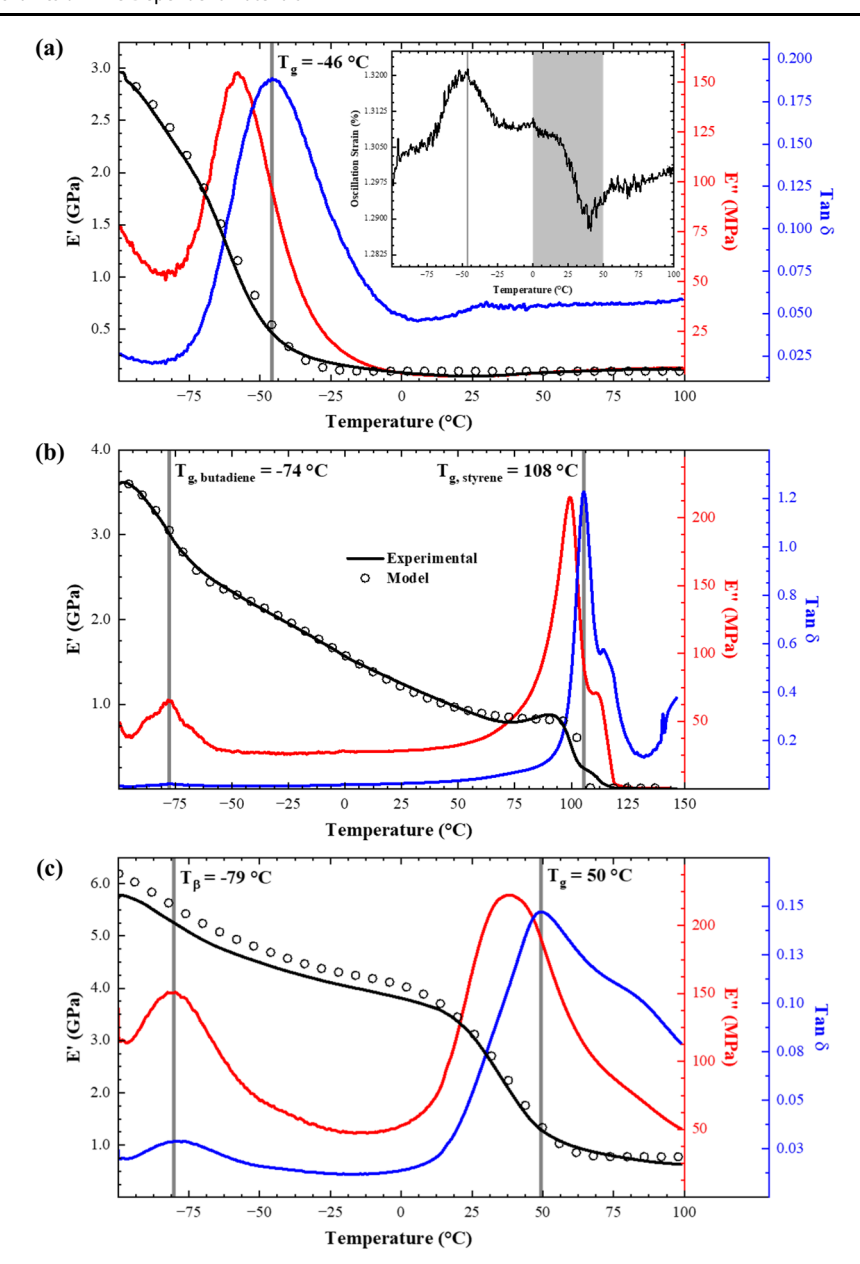


Fig. 3 Dynamic thermomechanical behavior of (a) TPU, (b) ABS, and (c) CFN printed samples, showing the mean (n = 3) storage and loss moduli, and $tan\delta$ as a function of temperature

at a frequency of 0.1 Hz while heating the sample at 3 °C/min. The results in **Fig. 3** indicate three noteworthy and synergetic observations: dynamic response, operating range, and temperature sensitivity. In general, these thermomechanical responses are typical of homo-, co-, and terpolymers, irrespective of reinforcement. It is worth noting that thermal transi-



tions in the forthcoming discussions are conventionally defined based on the peaks from the $tan\delta$ -temperature plots.

TPU reported a cryogenic glass transition temperature, consistent with its room temperature rubbery behavior, leading to a mechanically compliant response up to the terminal testing temperature. TPU reported a single thermal transition, i.e., glass transition, congruent with its molecular structure being homopolymer. The glass transition temperature (T_o) of TPU was found to be ca. -46 °C, limiting the glassy regime to cryogenic temperatures. The effective modulus $(E_{eff} = \sqrt{E'^2 + E''^2})$ of glassy TPU at -100 °C was 2960 \pm 101 MPa (average of three samples), descending to 51 ± 7 MPa at room temperature (23 °C) and plateauing thereafter at a slightly higher level (e.g., $E_{eff} = 117 \pm 8$ MPa at 100 °C). The latter observation (i.e., $E_{eff} = 89 \pm 13$ MPa for 23 °C < T < 100 °C) indicates that TPU exhibits an extended rubbery plateau and can be integrated into applications requiring a broad temperature operating range with high compliance, as discussed in a forthcoming section. Since the value of the loss factor $(tan\delta)$ is well below unity, it indicates that the relative degree of energy dissipation is lower than comparable materials with $tan\delta > 1$; hence, TPU might be suitable for high cushioning requirements. Here, the overall mechanical behavior of TPU is associated with local and global chain motions such that the energy-dissipating viscous elements have lower contributions to the dynamic properties of TPU. Notably, the thermomechanical spectrum shown in Fig. 3a agrees with the reported melting temperature of thermoplastic polyurethane (185–220 °C) (Stribeck et al. 2011; Frick and Rochman 2004) and the quasistatic modulus compared to the effective modulus at room temperature (Kim et al. 2017; Yanagihara et al. 2015). This foreseen utility is further substantiated by the peak of $tan\delta$, spreading over a broad temperature range from approximately -80 °C to 2 °C, evidencing relatively extended cushioning efficacy within the leathery and rubbery regimes. TPU continues to maintain the same values of the loss factor above 0 °C, showing nearly constant $tan\delta$ at 0.054 ± 0.003 up to the test terminal temperature.

It is imperative to highlight the notable dip in the $tan\delta$ plot of TPU for the temperature range 0 °C < T < 50 °C that transpired, by definition, from similar localized minima in the storage and loss moduli. The sudden reduction in the resistance to deformation metrics, i.e., moduli or $tan\delta$, is generally attributed to gradual sliding and slippage of the primary backbone as a function of temperature, owing to its linear polymer molecular structure, due to the dominance of the thermal relaxation energy over mechanical strain energy dissipation (Youssef 2021; Menard and Menard 2020; Lakes 2017). Remarkably, this trend coincides with the oscillating strain response shown in the inset of **Fig. 3a**. The strain-temperature plot indicates a pronounced valley, where the strain started to descend at 0 °C as a function of temperature, reaching a local minimum at ~34 °C before assuming a reversing trend reaching a plateau at ~55 °C. The reduction in the strain percentage ascertains the governance of macromolecular motions by the input thermal energy rather than the induced strain energy from the applied deflection amplitude.

Fig. 3b exemplifies the thermomechanical behavior of 3D printed samples using ABS, extending from −100 °C to the test terminal temperature of 150 °C. The latter was extended specifically for ABS to capture additional thermal transitions characteristic of this material (Kraus et al. 1967). The loss factor of ABS (**Fig. 3b**) shows two thermal transitions at −74 °C and 108 °C, corresponding to butadiene and styrene blocks, respectively (Kraus et al. 1967; Camelio et al. 1998; Cotten and Schneider 1963). Notably, the glass transition of copolymers of acrylonitrile was reported to range between 105 °C and 140 °C based on the molecular weight and processing conditions (Cotten and Schneider 1963); hence, it might have been slightly obscured or subsided by the thermal softening of ABS at the test terminal temperature. The thermal transition at 108 °C is associated with the styrene monomer, which



is expected to be at higher concentrations than other copolymers, i.e., acrylonitrile and butadiene (Kraus et al. 1967). The butadiene glass transition was found to be slightly higher than previous reports, probed at -74 °C herein while shown to be < -85 °C in (Kraus et al. 1967), which is attributed to the block length of the butadiene chains and their respective molecular weight within the ABS structure. The difference in T_g of butadiene is further substantiated by the faint peak in the $tan\delta$ plot, evidencing a low concentration of this monomer within the overall ABS macromolecule. In general, the results of glass transitions reported for ABS abide by the forecasts of the energy, volume, and mass model (Camelio et al. 1998). Furthermore, the storage modulus of ABS, shown in Fig. 3b, is in excellent agreement with previous reports of the dynamic behavior of this terpolymer (Dakshinamurthy and Gupta 2018; Yin et al. 2008). For example, it is well established that the operating temperature of ABS is extended up to ca. 80 °C, which is apodictic from the values of the storage modulus ranging from 3603 ± 992 MPa in the glass regime at -100 °C to 1.5 ± 0.8 MPa at the end of the testing range. The overshoot in the storage modulus before the glass transition of the styrene block is ascribed to stress relief, which was induced in the samples during the FFF 3D printing process (Menard and Menard 2020). The loss factor for ABS exemplifies a material with a higher relative degree of energy dissipation, indicating activation of viscous attenuation mechanisms. Hence, ABS might be more suitable for applications requiring higher dampening properties than TPU.

Finally, Fig. 3c shows the thermomechanical behavior of chopped carbon fiber reinforced nylon, which was 3D printed using the FFF printing process. Expectedly, the storage modulus, a measure of the material stiffness, is the highest of all tested samples, exceeding 5587 \pm 787 MPa at the onset testing temperature range. The effect of adding chopped carbon fibers on the mechanical behavior also transpired in the loss modulus and dampening factor as a function of temperature, like their influence on the storage modulus. Notably, the thermomechanical behavior of carbon-reinforced nylon herein trumps the results recently reported by Alarifi (Alarifi 2022). The differences between the results shown in Fig. 3c and (Alarifi 2022) are attributed to three possible sources: (1) the ratio of the reinforcing carbon fibers (\sim 8% herein vs. \sim 11% in (Alarifi 2022)), (2) processing parameters (e.g., printing speed and temperature), and (3) print orientation. The difference in the carbon fiber reinforcing ratio and the length of the carbon fiber (414 µm herein vs 119 µm in (Alarifi 2022)) contributes to the change in the material properties, as predicted by micromechanics models (Curtis et al. 1978; Christensen and Waals 1972). In (Alarifi 2022), Alarifi explored three printing orientations leaning towards unidirectionality, while the samples printed herein (also shown in Fig. 1) relied on alternating bidirectional printing to enhance mechanical performance. Otherwise, the thermomechanical performance reported in Fig. 3c agrees with the results of Alarifi (Alarifi 2022). However, since the measurements done herein were over a broad range of temperatures ($-100 \, ^{\circ}$ C to $100 \, ^{\circ}$ C), the loss factor plot captures two thermal transitions at -79 °C and 49 °C.

The thermal transitions of nylon have attracted assiduous research since its early stages of development using thermal (e.g., differential scanning calorimetry) and thermomechanical (e.g., dynamic mechanical analysis) methods (Forster 1968; Greco and Nicolais 1976; Gordon 1971). The manifestation of dual thermal transitions in nylons puzzled early researchers due to the amorphous molecular structure of nylons encompassing nonpolar hydrocarbons and amide groups with strong polarity (Gordon 1971; Boyer 1963). It is well accepted that the glass transition of nylons is between 40 °C and 70 °C, depending on the molecular arrangements and the processing conditions (Forster 1968; Greco and Nicolais 1976; Gordon 1971). The latter shifts the glass transition towards the higher bound due to interactions between the polar amide segments and the hydrogen bonding between the chains, especially



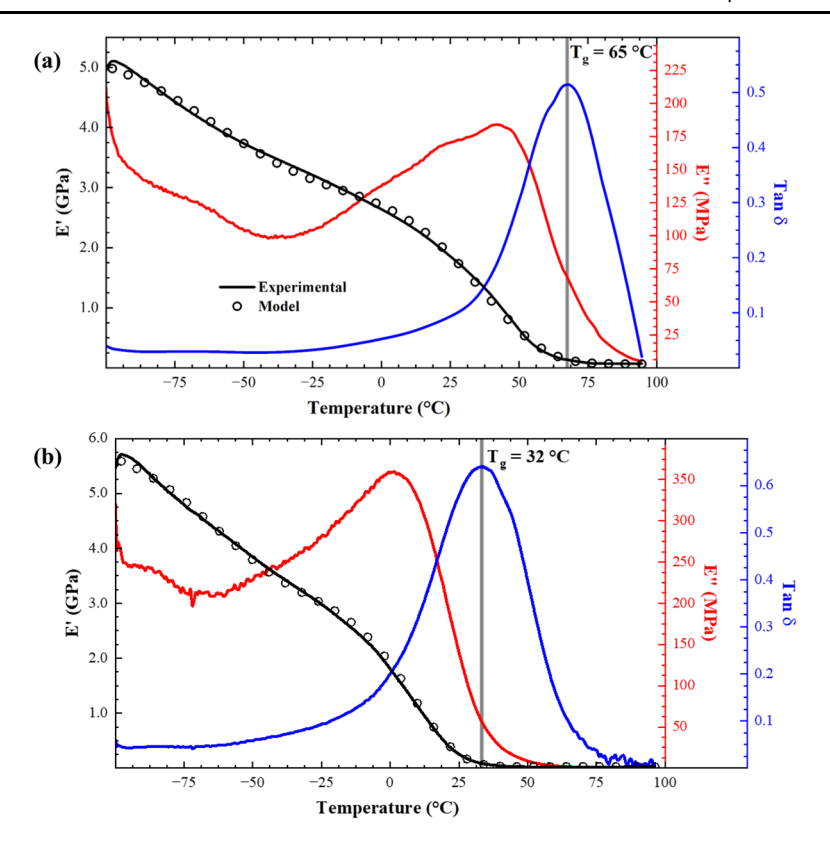


Fig. 4 Average dynamic thermomechanical response of (a) ABS-like and (b) rubber-like photocurable resins, showing the storage and loss moduli and the loss factor $(tan\delta)$ as a function of temperature

after thermal annealing. Notably, thermal annealing is a byproduct of the FFF printing process, where the filaments were heated up to 270 °C (well above melting temperature for nylon to achieve the proper flow of the carbon fiber-reinforced polymer through the printing nozzle), then cooled down rapidly upon deposition on the print plate that was heated to only 60 °C during the printing process. Therefore, 50 °C is taken as the glass transition of nylon, even though at lower temperatures the polymer exhibits pseudo-rubber behavior, as reported previously in (Greco and Nicolais 1976; Gordon 1971). Based on differential thermal analysis, Gordon postulated that the pseudo-rubber behavior below the glass transition temperature is associated with hydrogen bonding between the hydrocarbon chains being under dynamic equilibrium, giving rise to relative chain mobility and monotonic descent in the storage modulus as a function of temperature (Gordon 1971). The arising of an early thermal transition at -79 °C is then ascribed to the localized rearrangement of the hydrogen bonding (i.e., a second-order transition that only involves changes in the heat capacity without latent heat) (Youssef 2021; Gordon 1971).

3.2 Dynamic thermomechanical behavior of VPP printed materials

Fig. 4 plots the dynamic mechanical behavior of thermosetting ABS-like and rubber-like 3D printable, photocurable resins, including the storage modulus, the loss modulus, and



the $tan\delta$ as function of temperature (-100 °C < T < 100 °C). The commercial notation of 'ABS-like' and 'rubber-like' is based on the mechanical properties at room temperature, where the former imitates the mechanical properties of ABS (e.g., Fig. 3b) while the latter exhibits a relatively high loss modulus and loss factor, emulating rubbers. Indeed, the samples fabricated with the ABS-like resin reported a storage modulus of $E' = 1837 \pm 339$ MPa, a loss modulus of $E'' = 158 \pm 12$ MPa, and a loss factor of $tan\delta = 0.096 \pm 0.022$ at room temperature, which are comparable to the respective values for FFF printed counterparts (Fig. 3b). However, the dampening properties of ABS-like photocurable resins are inferior to FFF printed ABS counterparts since the loss factor is less than unity. The glass transition temperature for the ABS-like resin is 65 °C, limiting the operating range since the samples experienced a significant loss of stiffness after that. The storage modulus shows a monotonic descent below the defined glass transition, indicating the sensitivity of photo-polymerized macromolecule to a temperature that dynamically induces localized conformational mobility. The latter transpired in the loss modulus of the investigated resins, evidencing a dip in the glass regime due to a decrease in dissipated energy as the chains align (Silver et al. 2022). These results agree with recent reports on the viscoelastic properties of printable photocurable resins (Casado et al. 2022). Generally, the dynamic behavior of the rubber-like resin is consistent with the mechanistic expectations of rubbers as a function of temperature, resulting in a glass transition of 32 °C and rapid descent in the storage modulus in the denoted glassy regime. The viscoelastic response of rubber-like photocurable resin trumps FFF-printed TPU, exemplified by an extended temperature operating range. At the outset, it is imperative to note that while the dynamic properties of printable resins could be comparable to the FFF printed counterparts, the formers are plagued with their sensitivity to ultraviolet radiation, limiting their application to internal components or indoor usages.

3.3 Preliminary mechanics of 3D printed materials

The storage moduli of all 3D printed materials, irrespective of additive manufacturing methods, are fitted into a robust stiffness–temperature model (Mahieux and Reifsnider 2001). The motivation for exploring this phenomenological model stems from (1) the pronounced dependence of the storage modulus of polymers on the operating temperatures, evidencing several orders of magnitude reduction between the glassy and rubber regimes (Youssef 2021; Menard and Menard 2020; Lakes 2017), and (2) the facilitation of future engineering applications seeking robust mechanics relationships to be integrated into design analyses (Mahieux and Reifsnider 2001; Alasfar et al. 2022; Gunter 2006). As shown previously in Fig. 3 and Fig. 4, the storage modulus–temperature response exhibits multiple thermal transitions induced by molecular motions stemming from primary and secondary inter- and intramolecular bonds (Mahieux and Reifsnider 2001; Ashby and Jones 1986; Platzer 1969; Miller 1966). Mahieux and Reifsnider postulated a series of equations (modified in Eqn. (1)) based on simple spring–dashpot response, time–temperature equivalency in thermorheologically simple materials, the activation energies responsible for primary and secondary molecular bonds, and the Weibull distribution of the bond rupture associated with the latter.

$$E(T) = \sum_{i=1}^{n} (E_i - E_{i-1}) e^{\left(-\left(\frac{T}{T_i}\right)^{m_i}\right)} + E_T.$$
 (1)

The storage modulus E(T), as a function of the temperature of the investigated 3D printed polymers, was fitted into **Eqn.** (1) based on the number of thermal transitions (T_i) . E_i represents the storage modulus at the plateau region before a given thermal transition, E_T



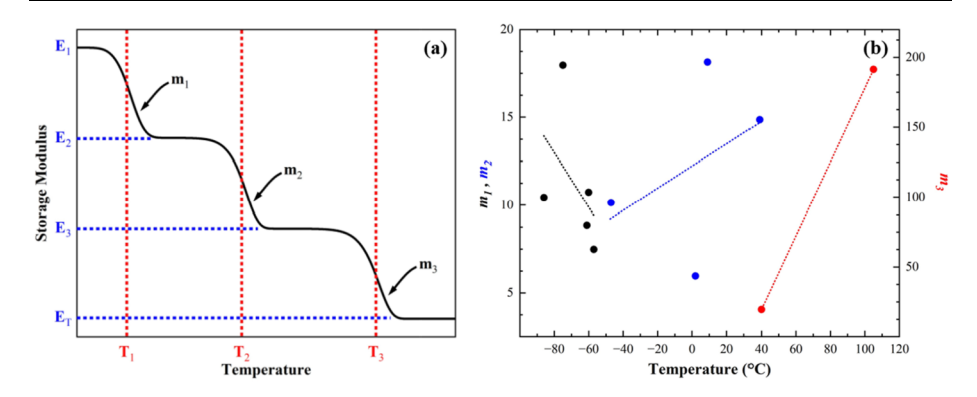


Fig. 5 (a) Schematic demonstrative of the curve fitting schema into Mahieux and Reifsnider model and (b) positive correlation between temperature and Weibull distribution coefficients, exemplifying effect of temperature on the participation rate of molecular motion

is the terminal modulus prior to the mechanical or thermal flow region, and m_i is the Weibull coefficient corresponding to the statistics of bond breakage at each transition, directly related to the degree of restriction in the molecular mobility. It is also imperative to note that the experimental characterization intentionally avoided the melt transition since this research emphasizes mechanical applications. Nonetheless, this approach can readily be extended to include additional thermal transitions, e.g., melting point, in future research to further optimize the additive manufacturing process or explore the utility of these polymers close to the thermal flow behavior. Fig. 5a is a demonstrative schematic of the physical correspondence of the fitting parameters with the experimental storage modulus as a function of temperature. Fig. 3 and Fig. 4 include the model results, showing reasonable agreement (evidenced by near unity correlation coefficients, as listed in Table 3) between the curve fitting and the experimental data while providing insights into the contributions of the molecular motions based on the resulting values of m_i .

Table 3 collates the curve fitting parameters, including the plateau moduli defining the onset stiffness preceding each transition, the transition temperature, and respective Weibull coefficients, deciphering the bond relaxation processes based on the chain participation and bond strength and stiffness. Mahieux and Reifsnider discussed the broad range of Weibull coefficients (m_i) based on the available conformational changes as a function of temperature (Mahieux and Reifsnider 2001). They foresaw a significant value of the Weibull coefficient for amorphous polymers due to the lack of considerable restrictions of molecular motion since the bond strength is bounded within a narrow distribution (Mahieux and Reifsnider 2001). Alternatively, Mahieux and Reifsnider argued that m_i assumes small values when conformational mobility is restricted by crosslinking or localized crystallinity (Mahieux and Reifsnider 2001). These mechanistic insights transpired herein for the investigated additively manufactured polymers based on the resolved values of the Weibull coefficients.

The resolved values of the Weibull distribution coefficients are plotted in **Fig. 5b** as a function of the corresponding transition temperatures, showing a correlation between the increase in temperature and the values for m_i . The latter observation persisted irrespective of the number of transitions, printing process, and type of polymer. The results corroborate the presumptions of Mahieux and Reifsnider, where low values of m_i coincided with low temperature, while the opposite was also confirmed (Mahieux and Reifsnider 2001). The low values of Weibull distribution coefficients indicate significant molecular restrictions given the glassy state of the polymers, where the molecular motions are confined to localized



 Table 3
 Stiffness-temperature model fitting parameters for investigated 3D printed material

	Transitions	E_1 (MPa)	T_1 (°C)	m_1	E_2 (MPa)	<i>T</i> ₂ (°C)	m_2	E_3 (MPa)	<i>T</i> ₃ (°C)	m_3	$E_T \eqno(MPa)$	R^2
FFF-TPU	1	3182	09-	10.73	,	,	ı	ı			76	0.99824
FFF-ABS	3	3871	-75	17.96	2809	2	5.96	797	105	191.33	12	0.99863
FFF-CFN	3	5953	98-	10.43	4664	-47	10.14	3514	40	19.54	775	0.99813
VPP-ABS-like resin	2	5347	-57	7.48	3024	39	14.85	,	1		2	0.99941
VPP-F69 resin	2	6033	-61	8.86	3215	6	18.14				29	0.99876



vibrations, bending and stretching, and side group perturbations (Mahieux and Reifsnider 2001). On the other hand, liberated molecular motions are associated with higher values of m_i , evidencing a greater level of chain participation in an overall reduction in resistance to deformation (i.e., low storage moduli) due to loosening the bond strength and stiffness at higher temperatures, increasing the available free volume and allowing gradual and significant chain motions. The results in **Table 3** and **Fig. 5b** are further synthesized as a function of printing materials to reconcile the values of the storage moduli and transition temperatures with the data discussed in §3.1 and §3.2. For example, the curve fitting parameters for FFF-CFN exemplify higher stiffness in the glassy regime substantiated by restrictive molecular motions based on the relatively low value of the Weibull coefficient. However, higher chain mobility coincides with increased values of the Weibull coefficient as the temperature increases (i.e., the value of m_3 for the third transition) such that FFF-CFN transitions away from the glassy region and into the rubbery regime. Finally, the terminal modulus of FFF-CFN is relatively higher than all other tested materials due to the reinforcement of the stiff, short carbon fibers. Similar conclusions are evidenced for the remaining printed materials, irrespective of the additive manufacturing process, giving rise to the mechanics of these polymers as a function of temperature and their corresponding molecular structures (discussed in §3.1 and §3.2).

At the outset, a note is warranted about the effect of the additive manufacturing process on the resulting mechanical properties, i.e., process–property interrelationship as a function of FFF and VPP, given the overarching focus of this research. While these 3D printing processes hinge on the same premise of layer-by-layer manufacturing, the performance of FFF-produced samples and parts hinges on the quality of the bonding lines between horizontally (i.e., within the same layer) and vertically (i.e., along the thickness direction) adjacent roads. The bonding quality depends on the processing parameters, including printing bed temperature, deposition speed, environment temperature, and part dimensions, which promote proper fusion of the polymer chains along the bond lines. On the other hand, the mechanical performance of VPP-fabricated samples depends on the viscosity of the resin during printing (affects reflow of the resin between layers and formation of bubbles and voids), the weight ratio of the photo-initiators, and the extent of post-processing steps. Future research by this group will focus on benchmarking the dynamic properties of 3D printed and conventionally fabricated samples.

3.4 Case study

The performance of walking and running shoes relies on the materials and structures of the soles, which comprise the insole in contact with the foot, providing cushioning and conformability, the midsole to mitigate the ground reaction force, and the outsole to reduce abrasion and increase traction (Uddin et al. 2020; Zahir Uddin et al. 2024). **Fig. 6a** is an illustration of the anatomy of the shoe soles, showing the in-, mid-, and outsole layers. Recently, 3D printing was used to mass produce walking and running shoes by prominent shoe manufacturers, seeking customization and tailor-ability by designing the different sole layers with unique structures and materials (Zolfagharian et al. 2021; Chhikara et al. 2023; Schwaar 2023). Selecting a specific structure depends on the manufacturing process, including resolution, speed, cost, and repeatability, which is a focus of a different research direction. However, matching materials for a sole layer can be demonstrated herein by considering the 3D printable polymers discussed above. In such consideration, walking and running shoes can be deployed in a wide range of temperatures, ranging from 0 °C (winter conditions), 23 °C (spring conditions), and 50 °C (hot summer conditions). The stiffness requirements hinge on the weight of the subject since body reaction force is a function of body



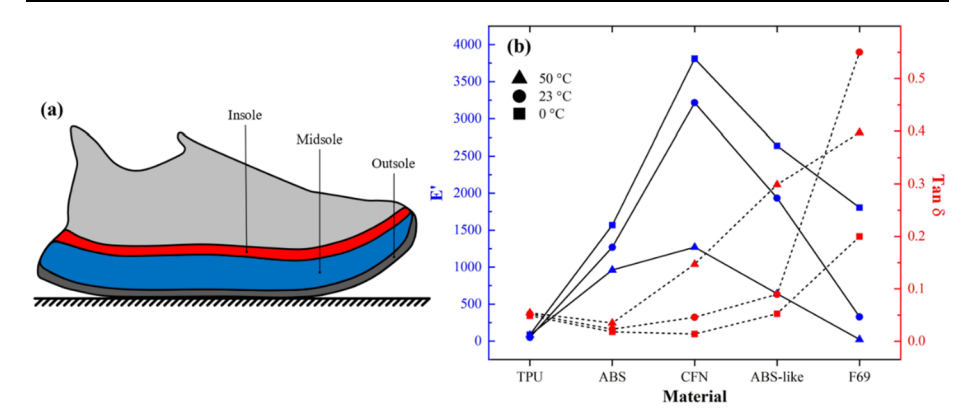


Fig. 6 (a) Schematic of the shoe sole structure, showing insole, midsole, and outsole, and (b) summary of the mechanical properties of investigated 3D printed materials within the temperature range foreseen in shoeing applications (at 0 °C, 23 °C, and 50 °C)

weight and moving speed (Zolfagharian et al. 2021). Hence, the storage moduli and loss factors for the additively manufactured polymers at three temperatures (0 °C, 23 °C, and 50 °C) assist in matching materials with loading and operating conditions. Fig. 6b summarizes the storage moduli and loss factors at the above-mentioned temperatures, evidencing a broad range of mechanical properties suitable for the design of walking and running shoes. The requirements of mechanical compliance with a relatively higher loss factor, i.e., rubber-like polymer, indicate VPP-F69 resins can be suitable for the additive manufacturing of outsoles. It is imperative to note that additional measurements of the wear resistance of VPP-F69 as a function of temperature and terrain are necessary further to substantiate the suitability of this material for outsoles. On the other hand, FFF-printable thermoplastic polyurethane, balancing between mechanical compliance and dampening (i.e., better cushioning), can be more suitable for insoles, leveraging these desirable mechanics and agility of the FFF 3D printing process. Finally, the midsole requires significant stiffness to provide rebounding and energy absorption, pointing to either FFF-CFN or VPP-ABS-like resin based on the level of structural tailoring, where the former might be conducive for simplified geometries, while the latter is suitable for higher degrees of customization, e.g., lattice or mathematically generated structures. Future research will emphasize the construction of multilayer soles and submitting these 3D printed structures to simulated and deployment conditions to ascertain the utility of additive manufacturing of these polymers in developing custom orthotics.

4 Conclusion

This research characterized the dynamic properties of additively manufactured polymers as a function of temperature, using materials with a broad range of thermomechanical behaviors. Three FFF-printable polymers (TPU, ABS, and chopped carbon fiber-reinforced nylon) and two photocurable polymers (ABS-like and flexible resins) were dynamically tested under a sinusoidal loading over a constant temperature ramp in a dual-cantilever configuration. Mechanical properties, including storage and loss moduli and the loss factor, were quantified as a function of temperature to ascertain the temperature sensitivity of each polymer. These dynamic properties yielded insight into the temperature ranges through which the polymers



exhibited structural stability and maximum damping behavior, delineating the operating envelope. A modified stiffness-temperature model provided additional mechanical insight into this behavior, correlating each thermal transition to the chain mobility at a molecular level. The fitted parameters for the model used in the research also provide additional context for the experimentally observed thermal transitions in each 3D printed polymer. Finally, the utility of the research was demonstrated by leveraging the temperature-governed dynamic properties in the design of 3D printed shoe sole layers deployed in a prescribed range of temperature environments, highlighting the application-driven motivation for characterizing the thermomechanical behavior of additive manufacturing materials.

Acknowledgements The authors acknowledge the support by the National Science Foundation under Grant No. 2035663. The authors are also grateful for internal funding from San Diego State University. Funding from the Department of Defense (W911NF1410039, W911NF1810477, and W911NF2210199) is also acknowledged. Support from San Diego State University is also acknowledged.

Author contributions All authors were responsible for writing (review and editing), data curation, formal analysis, investigation, visualization, figure preparation, and methodology. G.Y. is responsible for writing the original draft, conceptualization, project administration, resources, and funding acquisition.

Funding The research leading to these results is funded by the National Science Foundation under Grant No. 2035663 and from the Department of Defense (W911NF1410039, W911NF1810477, and W911NF2210199). The authors are also grateful for internal funding and support from San Diego State University. The authors have no competing interests to declare.

Data Availability Data will be made available upon request to the corresponding author.

Declarations

Competing interests The authors declare no competing interests.

References

- Adibeig, M.R., et al.: Quasi-static simulation and fatigue life estimation of fused filament fabrication of polylactic acid specimens using finite element method. J. Manuf. Process. **106**, 202–213 (2023)
- Ahn, S.H., et al.: Anisotropic material properties of fused deposition modeling ABS. Rapid Prototyping J. **8**(4), 248–257 (2002)
- Alarifi, I.M.: Investigation of the dynamic mechanical analysis and mechanical response of 3D printed nylon carbon fiber composites with different build orientation. Polym. Compos. **43**(8), 5353–5363 (2022)
- Alasfar, R.H., et al.: A review on the modeling of the elastic modulus and yield stress of polymers and polymer nanocomposites: effect of temperature, loading rate and porosity. Polymers 14(3), 360 (2022)
- Anandhan, S., et al.: Novel thermoplastic elastomers based on acrylonitrile-butadiene-styrene terpolymer (ABS) from waste computer equipment and nitrile rubber. Rubber Chem. Technol. **76**(5), 1145–1163 (2003)
- Anastasio, R., et al.: Characterization of ultraviolet-cured methacrylate networks: from photopolymerization to ultimate mechanical properties. Macromolecules **52**(23), 9220–9231 (2019)
- Andrady, A.L., et al.: Effects of increased solar ultraviolet radiation on materials. J. Photochem. Photobiol. B, Biol. **46**(1), 96–103 (1998)
- Andrady, A., et al.: Effects of UV radiation on natural and synthetic materials. Photochem. Photobiol. Sci. 22, 1–26 (2023)
- Ashby, M.F., Jones, D.R.H.: An Introduction to Microstructures, Processing and Design. No Title (1986)
- Bakhtiari, H., Aamir, M., Tolouei-Rad, M.: Effect of 3D printing parameters on the fatigue properties of parts manufactured by fused filament fabrication: a review. Appl. Sci. 13(2), 904 (2023)
- Boyer, R.F.: The relation of transition temperatures to chemical structure in high polymers. Rubber Chem. Technol. **36**(5), 1303–1421 (1963)
- Brans, K.: 3D printing, a maturing technology. In: IFAC Proceedings Volumes, vol. 46, pp. 468–472 (2013)



- Brighenti, R., et al.: Mechanical characterization of additively manufactured photopolymerized polymers. Mech. Adv. Mat. Struct. 30(9), 1853–1864 (2023)
- Camelio, P., et al.: Glass transition temperature calculations for styrene derivatives using the energy, volume, and mass model. Macromolecules 31(7), 2305–2311 (1998)
- Casado, J., et al.: 3D printable hybrid acrylate-epoxy dynamic networks. Eur. Polym. J. 173, 111256 (2022)
- Chantarapanich, N., et al.: Study of the mechanical properties of photo-cured epoxy resin fabricated by stereolithography process. Songklanakarin J. Sci. Technol. **35**(1) (2013)
- Chhikara, K., et al.: Development and effectiveness testing of a novel 3D-printed multi-material orthosis in nurses with plantar foot pain. Prosthesis 5(1), 73–87 (2023)
- Christensen, R., Waals, F.: Effective stiffness of randomly oriented fibre composites. J. Compos. Mater. 6(4), 518–532 (1972)
- Cotten, G., Schneider, W.: Transition temperatures in copolymers of acrylonitrile. Kolloid-Z. Z. Polym. 192, 16–21 (1963)
- Cuan-Urquizo, E., et al.: Characterization of the mechanical properties of FFF structures and materials: a review on the experimental, computational and theoretical approaches. Materials 12(6), 895 (2019)
- Curtis, P., Bader, M., Bailey, J.: The stiffness and strength of a polyamide thermoplastic reinforced with glass and carbon fibres. J. Mater. Sci. 13, 377–390 (1978)
- Dakshinamurthy, D., Gupta, S.: A study on the influence of process parameters on the viscoelastic properties of ABS components manufactured by FDM process. J. Inst. Eng. (India), Ser. C 99(2), 133–138 (2018)
- Deng, X., et al.: Mechanical properties optimization of poly-ether-ether-ketone via fused deposition modeling. Materials 11(2), 216 (2018)
- Desai, S.M., Sonawane, R.Y., More, A.P.: Thermoplastic polyurethane for three-dimensional printing applications: a review. Polym. Adv. Technol. 34(7), 2061–2082 (2023)
- Dizon, J.R.C., et al.: Mechanical characterization of 3D-printed polymers. Addit. Manuf. 20, 44-67 (2018)
- Dulieu-Barton, J., Fulton, M.: Mechanical properties of a typical stereolithography resin. Strain **36**(2), 81–87 (2000)
- Feng, J., et al.: Revealing molecular mechanisms of colorless transparent polyimide films under photo-oxidation. Polym. Degrad. Stab. 210, 110294 (2023)
- Forster, M.J.: Glass transition temperature of Nylon 6. Tex. Res. J. 38(5), 474-480 (1968)
- Frick, A., Rochman, A.: Characterization of TPU-elastomers by thermal analysis (DSC). Polym. Test. 23(4), 413–417 (2004)
- Gómez-García, D., et al.: Machinability of 3D printed peek reinforced with short carbon fiber. Comp. Part C Open Access 12, 100387 (2023)
- Gordon, G.A.: Glass transition in nylons. J. Polym. Sci., Part A-2, Polym. Phys. 9(9), 1693–1702 (1971)
- Greco, R., Nicolais, L.: Glass transition temperature in nylons. Polymer 17(12), 1049–1053 (1976)
- Gunter, E.: Designing with Plastics. Hanser Verlag, Munich (2006)
- Gurjar, D., Sharma, S., Sarkar, M.: A review on testing methods of recycled acrylonitrile butadiene-styrene. In: Materials Today: Proceedings, vol. 5, pp. 28296–28304 (2018)
- Hague, R., et al.: Materials analysis of stereolithography resins for use in rapid manufacturing. J. Mater. Sci. **39**(7), 2457–2464 (2004)
- Huynh, N.U., et al.: Property-map of epoxy-treated and as-printed polymeric additively manufactured materials. Int. J. Mech. Sci. **181**, 105767 (2020)
- Kim, D.S., Seo, W.H.: Ultraviolet-curing behavior and mechanical properties of a polyester acrylate resin. J. Appl. Polym. Sci. **92**(6), 3921–3928 (2004)
- Kim, K., et al.: 3D printing of multiaxial force sensors using carbon nanotube (CNT)/thermoplastic polyurethane (TPU) filaments. Sens. Actuators A, Phys. 263, 493–500 (2017)
- Kraus, G., Childers, C., Gruver, J.: Properties of random and block copolymers of butadiene and styrene. I. Dynamic properties and glassy transition temperatures. J. Appl. Polym. Sci. 11(8), 1581–1591 (1967)
- Kuenstler, A.S., et al.: Vat photopolymerization additive manufacturing of tough, fully recyclable thermosets. ACS Appl. Mater. Interfaces **15**(8), 11111–11121 (2023)
- Kumar, S., et al.: Fused filament fabrication: a comprehensive review. J. Thermoplast. Compos. Mater. 36(2), 794–814 (2023)
- Lakes, R.S.: Viscoelastic Solids (1998). CRC Press, Boca Raton (2017)
- Lantean, S., et al.: Magnetoresponsive devices with programmable behavior using a customized commercial stereolithographic 3D printer. Adv. Mater. Technol. **7**(11), 2200288 (2022)
- Laureto, J.J., Pearce, J.M.: Anisotropic mechanical property variance between ASTM D638-14 type I and type IV fused filament fabricated specimens. Polym. Test. 68, 294–301 (2018)
- Ligon, S.C., et al.: Polymers for 3D printing and customized additive manufacturing. Chem. Rev. 117(15), 10212–10290 (2017)
- Mahieux, C.A., Reifsnider, K.L.: Property modeling across transition temperatures in polymers: a robust stiffness-temperature model. Polymer 42(7), 3281–3291 (2001)



- Malley, S., Newacheck, S., Youssef, G.: Additively manufactured multifunctional materials with magnetoelectric properties. Addit. Manuf. 47, 102239 (2021)
- Menard, K.P., Menard, N.: Dynamic Mechanical Analysis. CRC Press, Boca Raton (2020)
- Miller, M.L.: The structure of polymers (1966). (No Title)
- Naik, D.L., Kiran, R.: On anisotropy, strain rate and size effects in vat photopolymerization based specimens. Additive Manufacturing 23, 181–196 (2018)
- Namvar, N., et al.: Bio-inspired design, modeling, and 3D printing of lattice-based scale model scooter decks. Int. J. Adv. Manuf. Technol. **126**(7), 2887–2903 (2023)
- Naveen, R., et al.: An investigation on effect of ultraviolet (UV) rays on mechanical properties of epoxy laminates. Mater. Today Proc. (2023)
- Nugraha, A.D., Syahril, M., Muflikhun, M.A.: Excellent performance of hybrid model manufactured via additive manufacturing process reinforced with GFRP for sport climbing equipment. Heliyon **9**(3), e14706 (2023)
- Onwubolu, G.C., Rayegani, F.: Characterization and optimization of mechanical properties of ABS parts manufactured by the fused deposition modelling process. Int. J. Manuf. Eng. **2014**, 1–13 (2014)
- Pachauri, S., Gupta, N.K., Gupta, A.: Influence of 3D printing process parameters on the mechanical properties of polylactic acid (PLA) printed with fused filament fabrication: experimental and statistical analysis. Int. J. Interact. Des. Manuf., 1–19 (2023)
- Patterson, A.E., et al.: Fracture testing of polymer materials processed via fused filament fabrication: a survey of materials, methods, and design applications. Prog. Addit. Manuf. 6(4), 765–780 (2021)
- Platzer, N.: Progress in polymer engineering. Ind. Eng. Chem. **61**(5), 10–30 (1969)
- Prashar, G., Vasudev, H., Bhuddhi, D.: Additive manufacturing: expanding 3D printing horizon in industry 4.0. Int. J. Interact. Des. Manuf. 17(5), 2221–2235 (2023)
- Ramya, A., Vanapalli, S.L.: 3D printing technologies in various applications. Int. J. Mech. Eng. Technol. 7(3), 396–409 (2016)
- Randhawa, K.S., Patel, A.: The effect of environmental humidity/water absorption on tribo-mechanical performance of polymers and polymer composites—a review. Ind. Lubr. Tribol. **73**(9), 1146–1158 (2021)
- Reich, M.J., et al.: Mechanical properties and applications of recycled polycarbonate particle material extrusion-based additive manufacturing. Materials **12**(10), 1642 (2019)
- Riechert, V., et al.: Rheological properties and UV photo-oxidation of montmorillonite-filled random propylene-ethylene copolymers. Polym. Bull. **80**(4), 3981–4004 (2023)
- Rodríguez, J.F., Thomas, J.P., Renaud, J.E.: Mechanical behavior of acrylonitrile butadiene styrene (ABS) fused deposition materials. Experimental investigation. Rapid Prototyping J. 7(3), 148–158 (2001)
- Sabatini, F., et al.: A thermal analytical study of LEGO® bricks for investigating light-stability of ABS. Polymers 15(15), 3267 (2023)
- Sărăndan, S.O.: Contributions regarding the development of cellular structures destined for sports equipment (2022)
- Schwaar, C.: 3D Printed Shoes: The Cream of the Crop of 2023 (2023)
- Senna, S.: Design, 3D printing and characterisation of bending-dominated lattice structures for energy absorption in sports equipment (2019)
- Shojib Hossain, M., et al.: Improving tensile mechanical properties of FDM-manufactured specimens via modifying build parameters. In: 2013 International Solid Freeform Fabrication Symposium (2013). University of Texas at Austin
- Shojib Hossain, M., et al.: Improved mechanical properties of fused deposition modeling-manufactured parts through build parameter modifications. J. Manuf. Sci. Eng. 136(6), 061002 (2014)
- Silver, F.H., Gonzalez-Mercedes, M., Mesica, A.: A rapid method to noninvasively measure the viscoelastic properties of synthetic polymers using mechanical vibrations and photonics. Photonics **9**(12), 925 (2022)
- Sola, A., et al.: Open challenges in tensile testing of additively manufactured polymers: a literature survey and a case study in fused filament fabrication. Polym. Test. 117, 107859 (2023)
- Song, Y., et al.: An overview of selective laser sintering 3D printing technology for biomedical and sports device applications: processes, materials, and applications. Opt. Laser Technol. 171, 110459 (2024)
- Sood, A.K., Ohdar, R.K., Mahapatra, S.S.: Experimental investigation and empirical modelling of FDM process for compressive strength improvement. J. Adv. Res. 3(1), 81–90 (2012)
- Stribeck, N., et al.: Structure and mechanical properties of an injection-molded thermoplastic polyurethane as a function of melt temperature. Macromol. Chem. Phys. **212**(20), 2234–2248 (2011)
- Svetlana, T., et al.: Flexural quasi-static and fatigue behaviours of fused filament deposited PA6 and PA12 polymers. Int. J. Adv. Manuf. Technol. 117(7), 2041–2048 (2021)
- Tan, L.J., Zhu, W., Zhou, K.: Recent progress on polymer materials for additive manufacturing. Adv. Funct. Mater. 30(43), 2003062 (2020)



- Uddin, M.S., et al.: Evaluating mechanical properties and failure mechanisms of fused deposition modeling acrylonitrile butadiene styrene parts. J. Manuf. Sci. Eng. 139(8), 081018 (2017)
- Uddin, K.Z., et al.: Gradient optimization of multi-layered density-graded foam laminates for footwear material design. J. Biomech. 109, 109950 (2020)
- Vidakis, N., Petousis, M., Kechagias, J.: A comprehensive investigation of the 3D printing parameters' effects on the mechanical response of polycarbonate in fused filament fabrication. Prog. Addit. Manuf. 7(4), 713–722 (2022)
- Wang, Y., et al.: Acoustic-assisted 3D printing based on acoustofluidic microparticles patterning for conductive polymer composites fabrication. Addit. Manuf. 60, 103247 (2022)
- Wineman, A.S., Rajagopal, K.R.: Mechanical Response of Polymers: An Introduction. Cambridge University Press, Cambridge (2000)
- Wittbrodt, B., Pearce, J.M.: The effects of PLA color on material properties of 3-D printed components. Addit. Manuf. 8, 110–116 (2015)
- Xiang, Y., et al.: Mechanical characterization and constitutive modeling of visco-hyperelasticity of photocured polymers. Addit. Manuf. 36, 101511 (2020)
- Yadav, A., et al.: Fused filament fabrication: a state-of-the-art review of the technology, materials, properties and defects. Int. J. Interact. Des. Manuf. 17(6), 2867–2889 (2023)
- Yanagihara, Y., et al.: Relationship between modulus and structure of annealed thermoplastic polyurethane. Mater. Today Commun. **2**, e9–e15 (2015)
- Yankin, A., et al.: Optimization of printing parameters to enhance tensile properties of ABS and nylon produced by fused filament fabrication. Polymers 15(14), 3043 (2023)
- Yin, Z.N., Fan, L.F., Wang, T.J.: Experimental investigation of the viscoelastic deformation of PC, ABS and PC/ABS alloys. Mater. Lett. **62**(17), 2750–2753 (2008)
- Yousif, E., et al.: Photo-physical and morphological study of polymers: a review. Phys. Chem. Res. 11(2), 409–424 (2023)
- Youssef, G.: Applied Mechanics of Polymers: Properties, Processing, and Behavior. Elsevier, Amsterdam (2021)
- Youssef, G., et al.: Multifunctional fused deposition modeled acrylonitrile butadiene styrene-based structures with embedded conductive channels. J. Eng. Mater. Technol. 143(1), 011001 (2021)
- Zahir Uddin, K., et al.: In-plane Density Gradation of Shoe Midsoles for Optimized Cushioning Performance (2024). e-prints, arXiv:2401.06940
- Zaldivar, R., et al.: Influence of processing and orientation print effects on the mechanical and thermal behavior of 3D-printed ULTEM® 9085 material. Addit. Manuf. 13, 71–80 (2017)
- Zolfagharian, A., et al.: Custom shoe sole design and modeling toward 3D printing. Int. J. Bioprinting 7(4) (2021)

Publisher's Note Springer Nature remains neutral with regard to jurisdictional claims in published maps and institutional affiliations.

Springer Nature or its licensor (e.g. a society or other partner) holds exclusive rights to this article under a publishing agreement with the author(s) or other rightsholder(s); author self-archiving of the accepted manuscript version of this article is solely governed by the terms of such publishing agreement and applicable law.

